




## Article

# Effect of Sun Drying on Phytoconstituents and Antiviral Activity of Ginger against Low-Pathogenic Human Coronavirus

Yasmin A. Elkhawas <sup>1,\*</sup>, Haidy A. Gad <sup>2</sup>, Manar O. Lashkar <sup>3</sup>, Roaa M. Khinkar <sup>3</sup>, Mohmmad Y. Wani <sup>4</sup> and Noha Khalil <sup>1</sup>

<sup>1</sup> Department of Pharmacognosy and Medicinal Plants, Faculty of Pharmacy, Future University in Egypt, Cairo 11835, Egypt

<sup>2</sup> Department of Pharmacognosy, Faculty of Pharmacy, Ain Shams University, Cairo 11566, Egypt

<sup>3</sup> Department of Pharmacy Practice, Faculty of Pharmacy, King Abdulaziz University, Jeddah 21589, Saudi Arabia

<sup>4</sup> Department of Chemistry, College of Science, University of Jeddah, Jeddah 21589, Saudi Arabia

\* Correspondence: yasmien.alaa@fue.edu.eg; Tel.: +20-11-4163-3982

**Abstract:** Rhizomes of ginger are commonly used as a spice and for home remedies in either fresh or dry form. This study aimed to assess the effect of sun drying on the volatile constituents, total phenolic and flavonoid content, and the antiviral activity of ginger against low-pathogenic human coronavirus. The antiviral effect of the major volatile compounds was predicted through molecular docking. GC/MS was employed for profiling the volatile constituents of both fresh and dry ginger oils. Moreover, chemometric analysis was applied to discriminate between fresh and dry ginger and to investigate the correlation between their volatile constituents and the antiviral activity using principal component analysis (PCA) and partial least-squares regression (PLS-R). GC/MS analysis revealed that the major effects of the drying process were an increase in  $\alpha$ -curcumene and  $\beta$ -sesquiphellandrene. Moreover, total phenolic and flavonoid contents of dried ginger decreased considerably. A PCA score plot revealed significant discrimination between fresh and dry ginger, with  $\alpha$ -curcumene and 4-thujanol identified as the main discriminating markers. These findings were validated by in silico molecular docking studies, which revealed that the compounds under consideration had good drug-like characteristics. Thus, ginger is rich in valuable phytoconstituents which showed promising therapy in viral infections such as COVID-19.

**Keywords:** sun-dried ginger; GC/MS; coronavirus;  $\alpha$ -Curcumene; chemometrics; molecular docking; drug discovery; industrial development



**Citation:** Elkhawas, Y.A.; Gad, H.A.; Lashkar, M.O.; Khinkar, R.M.; Wani, M.Y.; Khalil, N. Effect of Sun Drying on Phytoconstituents and Antiviral Activity of Ginger against Low-Pathogenic Human Coronavirus. *Agronomy* **2022**, *12*, 2763. <https://doi.org/10.3390/agronomy12112763>

Academic Editors: Laura Siracusa and Rosa Palmeri

Received: 9 October 2022

Accepted: 3 November 2022

Published: 6 November 2022

**Publisher's Note:** MDPI stays neutral with regard to jurisdictional claims in published maps and institutional affiliations.



**Copyright:** © 2022 by the authors. Licensee MDPI, Basel, Switzerland. This article is an open access article distributed under the terms and conditions of the Creative Commons Attribution (CC BY) license (<https://creativecommons.org/licenses/by/4.0/>).

## 1. Introduction

Ginger is a highly valuable crop because it contains oleoresin and volatile oil. It is one of the most extensively cultivated spices for export on a business scale, and it is highly valued in the global market for its pungency, scent, and high oleoresin content. The quality of ginger rhizome in the world market depends mainly on its pungency, aroma, essential oils, and oleoresin. These chemical and physical characteristics are affected by many aspects, such as maturity, variety, and processing conditions [1]. Volatile oils are ethereal fragrant liquids derived from various plant parts such as fruits, flowers, leaves, bark, seeds, and roots. They are stored in secretory glands such as vittae, epidermic cells, and glandular trichomes [2]. They are formed of a mixture of monoterpenes, sesquiterpenes, and their oxygenated derivatives through isoprenoid routes. These secondary bioactive metabolites participate in plants' defense systems against biotic and abiotic stress [3]. Apart from their numerous uses in pharmaceutical, food, and cosmetic manufacturing, they are also known for their pharmacological activities (antibacterial, antifungal, antioxidant, anticancer, antiviral, analgesic, anti-inflammation, and antispasmodic) [4–7].

Ginger plays a vital role in Indian, Chinese, and Japanese medicine as it has established a good reputation in treating many disorders. Many studies have reported that ginger has antioxidant, hypocholesterolemic, and anti-obesity properties [8,9]. Most ginger is frequently shipped from production locations in processed form as a dried ginger powder [10]. Drying is important in the post-harvesting process for preserving crops and prolonging the food shelf lifetime [11]. Removing moisture using the appropriate drying method can prevent deterioration reactions and decay [12]. The most common traditional method for food preservation performed in many urban and rural areas of developing countries is the sun drying of various crops. Considering the rural population's low income, the comparatively large investment for energy-based dryers such as the pulsed vacuum, the cabinet dryer, the air dryer, the microwave, infrared dehydration, and freeze drying, remains a barrier to widespread adoption [13].

Natural products have traditionally played an important part in the medication development process for a variety of diseases, resulting in the screening of such medicines to combat emerging mutants of the coronavirus [14]. Ginger, a well-known herbal plant, served as a good candidate due to its richness of many biologically active compounds and a broad array of pharmacological activities, such as anti-inflammatory, antioxidant, anticancer, antiviral, and antimicrobial activities [15,16].

Coronaviruses, a broad family of viruses, cause various illnesses ranging from the common cold to severe acute respiratory syndrome (SARS). In 2003, SARS-CoV spread to five continents, killing 10% of those infected [17,18]. Another major health threat to the entire world is SARS-CoV-2, also known as COVID-19. The SARS-CoV-2 virus, discovered in Wuhan, China, caused a worldwide pandemic [19]. COVID-19 infection spread quickly among humans, prompting the WHO to proclaim it a pandemic [20–22]. Apart from the development of vaccines, the development of a new molecule that could combat this virus and overcome the COVID-19 pandemic is critical.

While the success of vaccines to combat COVID-19 infection is undeniable, negative attitudes towards vaccines, an uncertainty or unwillingness to receive vaccines, concerns about future side effects, and reduced efficacy of vaccines owing to emerging variants of concern are a large challenge [23,24]. The development of alternative treatment modalities is an effective strategy to contain or combat this viral infection. Plants have been a great source from which biologically important molecules have been identified and isolated for successfully treating many diseases and ailments [25,26]. Several studies have been undertaken to identify bioactive components from plants and plant sources that have the potential to inhibit the proliferation of the virus [27–29].

This study aimed to assess the effect of sun drying on the volatile constituents, total phenolics, and total flavonoid content, as well as demonstrate how sun drying affected the *in vitro* antiviral activity of ginger against SARS-CoV-2, together with a prediction of the antiviral effect of the major volatile compounds by using molecular docking. Chemometrics was applied as a multivariate tool to find similarities and differences between fresh and dry ginger and determine the relationship between the volatile compounds and antiviral activity.

## 2. Materials and Methods

### 2.1. Plant Material

Fresh ginger rhizomes were gathered from the medical farm of the Arab Company of Pharmaceuticals and Medicinal Plants (Mepaco-Medifood), El Sharqiya, Egypt. They were kindly authenticated by Dr. Therese Labib, Taxonomist and ex-manager of the Botanical Orman Garden, Giza, Egypt. Voucher specimens (G12-22) were kept at the Pharmacognosy research lab at the Faculty of Pharmacy, Future University in Egypt.

### 2.2. Isolation of Volatile Oil

Under running water, the entire mature rhizomes were thoroughly washed and drained to remove surface dust and unwanted materials. The drained rhizomes were

divided into two halves. The first half was peeled by a knife and ground. The second half was subjected to sun drying after peeling in the open air for 14 days until completely dry (constant weight for 3 days). Rhizomes were ground to 20–40 mesh-size particles before being hydro-distilled for 5 h in a Clevenger-type device to extract the oils. The oils were dried over anhydrous  $\text{Na}_2\text{SO}_4$ .

$$\text{Essential oil yield (\% v/w)} = [\text{Volume of essential oil (mL)}/\text{Weight of plant (g)}] \times 100$$

### 2.3. GC-MS Analysis

Using a Shimadzu GC MS-QP2010 (Tokyo, Japan) equipped with Rtx-5MS fused bonded column (30 m  $\times$  0.25 mm i.d.  $\times$  0.25  $\mu\text{m}$  film thickness) (Restek, Bellefonte, PA, USA) and a split-splitless injector, the mass spectrum was recorded [30]. The capillary column was directly coupled to a quadrupole mass spectrometer (SSQ 7000; Thermo-Finnigan, Bremen, Germany). The initial column temperature was kept at 45  $^\circ\text{C}$  for 2 min (isothermal), programmed to 300  $^\circ\text{C}$  at a rate of 5  $^\circ\text{C}/\text{min}$  and kept constant at 300  $^\circ\text{C}$  for 5 min (isothermal). The helium carrier gas flow rate was 1.41 mL/min. The injector temperature was 250  $^\circ\text{C}$ . The mass spectrum was recorded by applying a filament emission current of 60 mA, ionization voltage of 70 eV, and 200  $^\circ\text{C}$  ion source. A diluted sample (1% v/v) was injected with split mode with a split ratio of 1:15.

### 2.4. Determination of Total Phenolic Content

Ginger was chopped into pieces independently to make the methanol extract. Folin-Ciocalteu reagents were used to determine the total phenolic content, with analytical grade gallic acid serving as the standard, with the calibration curve shown in Figure S1 [31]. Briefly, the procedure consisted of mixing 10  $\mu\text{L}$  of sample/standard with 100  $\mu\text{L}$  of Folin-Ciocalteu reagent (diluted 1:10) in a 96-well microplate. Then, 80  $\mu\text{L}$  of 1 M  $\text{Na}_2\text{CO}_3$  was added and incubated at room temperature (25  $^\circ\text{C}$ ) for 20 min in the dark. At the end of incubation time the resulting blue complex color was measured at 630 nm. Data are represented as means  $\pm$  SD.

### 2.5. Determination of Total Flavonoid

The total flavonoid content was investigated as defined by [32] with minor modifications to be carried out in microplates. Rutin was used as standard flavonoid with the calibration curve shown in Figure S2. Briefly, 15  $\mu\text{L}$  of sample/standard was placed in a 96-well microplate, then 175  $\mu\text{L}$  of methanol was added, followed by 30  $\mu\text{L}$  of 1.25%  $\text{AlCl}_3$ . Finally, 30  $\mu\text{L}$  of 0.125 M  $\text{C}_2\text{H}_3\text{NaO}_2$  was added and incubated for 5 min. At the end of incubation time, the resulting yellow color was measured at 420 nm. Data are represented as means  $\pm$  SD.

### 2.6. Determination of Antiviral by Crystal Violet Method on Low Pathogenic Corona Virus

The crystal violet method was used to evaluate the antiviral activity and cytotoxicity assays using the recent study on the cytopathic (CPE) inhibition effect [33]. According to [34], the percentage of antiviral activities of the tested samples were calculated using the following equation: antiviral activity = [(mean optical density of cell controls – mean optical density of virus controls)/(optical density of test – mean optical density of virus controls)]  $\times$  100%. Using GraphPad PRISM software (Graph-Pad Software, San Diego, CA, USA), the results of the 50% cytotoxic concentrations ( $\text{CC}_{50}$ ) and the 50% inhibitory concentration ( $\text{IC}_{50}$ ) were investigated.

### 2.7. Molecular Docking

Molecular docking is a simulation technique that finds the optimal fit between the active sites of certain targets and the ligands. This process necessitates arranging the 3D coordinate space on the target's binding site, calculating the binding affinity of the created complex, and developing the subsequent orientation of a molecule on the ligand's binding

site. The biggest negative value represents binding affinity sensitivity, signifying the most suitable conformation of the created complex [35]. The predicted pharmacokinetic parameters and other physicochemical properties, often known as Lipinski's filters, are important for both *in silico* and *in vitro* evaluation of drug-like properties [36–38]. Molecules that do not show good pharmacokinetic properties and do not obey Lipinski's filters fail in the later stages of the drug development process. The crystal structure of the COVID-19 main protease in complex with an inhibitor N3 was obtained from Protein Data Bank (<https://www.rcsb.org/structure/6LU7>, accessed on 15 May 2022) with the PDB ID 6LU7, resolution: 2.16 Å. For the docking analysis, Molecular Operating Environment (MOE) was used [39]. In this investigation, the lead molecule's free energies and binding modes towards the target proteins were determined. Firstly, water molecules were eliminated from the crystal structures of target proteins, leaving only one chain essential for binding. Secondly, the reference ligand was co-crystallized, the protein structures were protonated, and hydrogen atoms were hidden. Finally, the MMFF94x force field was utilized to decrease the energy, and the binding pocket of the target protein was well-defined with predefined MOE settings. ChemBioDraw Ultra 14.0 was applied to illustrate the structure of the molecules 4-Thjanol, Neral, Geranial, Camphene,  $\alpha$ -Curcumene, Zingiberene,  $\gamma$ -Cadinene,  $\beta$ -Bisabolene, and  $\beta$ -Sesquiphellandrene (1N1–1N9), which were saved in SDF formats. Subsequently, the stored files were launched using MOE software, and 3D structures were protonated. The MMFF94x force field was then used to reduce the energy of the molecules. Validation processes for the target receptor were conducted by running the docking process for only the co-crystallized ligand. Valid performance is shown by low RMSD values between docked and crystal conformations. The output from the MOE software was further evaluated and visualized employing both MOE and Discovery Studio 4.0 software.

### 2.8. Chemometric Analysis

Chemometric analysis was performed on the GC-MS results. Principal component analysis (PCA) was utilized as an initial step for data examination to present an overview of all sample discrepancies and to recognize markers accountable for their dissimilarity. A quantitative calibration model, partial least-squares (PLS), was designed to find a correlation between the volatile constituents (GC/MS peak areas) (X) matrix and the antiviral activity (Y) matrix. In this state, there was no division of data into the model and test sets as only 6 samples were assessed (small data set). PCA and PLS were performed using CAMO's Unscrambler<sup>®</sup> X 10.4 software (Computer-Aided Modeling, AS, Oslo, Norway).

## 3. Results and Discussion

### 3.1. Effect of Sun Drying on the Yield and Composition of Ginger Volatile Oil

The fresh and dried volatile oil yields were  $1.51 \pm 0.244\%$  *v/w* and  $2.75 \pm 0.326\%$  *v/w*, respectively. The oils had a characteristic pale-yellow color and pungent aromatic odor. GC-MS Total Ion Chromatograms (TIC) of the ginger oils compounds are shown in Figure S3. The baseline of the total ion diagram showed a steady and good separation of individual peaks with no supersaturation state. The composition of fresh and dried ginger volatile oils is displayed in Table 1. In the fresh and dried ginger analysis, 45 and 43 aroma compounds were extracted and identified. In fresh ginger volatile oils, 11 compounds were oxygenated monoterpenes, 4 monoterpenes, 11 sesquiterpene hydrocarbons, 10 oxygenated sesquiterpenes, and 9 miscellaneous, whereas in dried ginger volatile oil, 14 compounds were oxygenated monoterpenes, 3 monoterpenes, 14 sesquiterpene hydrocarbons, 5 oxygenated sesquiterpenes, and 7 miscellaneous. The main compounds of the dried ginger volatile oil were  $\alpha$ -Curcumene (28.19%), followed by  $\beta$ -Sesquiphellandrene (15.06%), Zingiberene (14.84%),  $\beta$ -Bisabolene (11.64%) and  $\gamma$ -Cadinene. The relatively high amount of Zingiberene and  $\beta$ -sesquiphellandrene justify the odor of the dried ginger, matching the results of [40]. In comparison, the major compounds of fresh ginger volatile oil were  $\alpha$ -Curcumene (14.23%), followed by 4-Thujanol (9.94%). The sun drying method caused a change in the volatile constituents, in which the percentage of sesquiterpenes com-

pounds ( $\alpha$ -Curcumene, Eudesma-4(14),11-diene, Zingiberene,  $\gamma$ -Cadinene,  $\beta$ -Bisabolene,  $\alpha$ -Selinene, and  $\beta$ -Sesquiphellandrene) showed a significant rise while the monoterpenes camphene reduced considerably. This could be ascribed to the synthesis of isomerization of compounds and short-chain alkenes. Additionally, many acetates were detected in sun-dried ginger only, such as citronellol acetate, nerol acetate, and nerolidyl acetate. This may be credited to prolonged exposure to oxygen causing the esterification of alcohols to their corresponding esters, which was confirmed by [41].

**Table 1.** Chemical composition and classifications of compounds of both fresh and dried ginger volatile oil.

	<sup>a</sup> Compound	<sup>b</sup> Retention Index (RI)	Fresh Ginger	Dry Ginger	Identification
1	$\beta$ -Butoxyethanol	665	1 $\pm$ 0.040	1.01 $\pm$ 0.064	MS, RI
2	<i>n</i> -Caproaldehyde	806	0.4 $\pm$ 0.016	0.26 $\pm$ 0.0163	MS, RI
3	2-Methyl-2-hepten-6-on	938	0.59 $\pm$ 0.020	-	MS, RI
4	$\beta$ -Pinene	943	0.27 $\pm$ 0.048	-	MS, RI
5	$\alpha$ -Pinene	948	1.99 $\pm$ 0.008	-	MS, RI
6	Camphene	952	7 $\pm$ 0.326	0.51 $\pm$ 0.008	MS, RI
7	$\beta$ -Myrcene	958	2.91 $\pm$ 0.040	-	MS, RI
8	5-Hepten-2-one, 6-methyl-	966	-	0.61 $\pm$ 0.016	MS, RI
9	Octanal	1005	0.37 $\pm$ 0.044	-	MS, RI
10	<i>o</i> -Cymene	1015	-	0.24 $\pm$ 0.040	MS, RI
11	Eucalyptol	1022	-	1 $\pm$ 0.408	MS, RI
12	4-Thujanol	1041	9.94 $\pm$ 0.048	-	MS, RI
13	Cryptone	1069	0.87 $\pm$ 0.098	-	MS, RI
14	Benzene, (2-methyl-1-propenyl)-	1077	-	0.39 $\pm$ 0.008	MS, RI
15	<i>trans</i> -Verbenol	1082	-	0.17 $\pm$ 0.020	MS, RI
16	Linalool	1090	-	0.81 $\pm$ 0.016	MS, RI
17	2-Nonanol	1092	0.18 $\pm$ 0.032	0.29 $\pm$ 0.032	MS, RI
18	Citronellal	1125	0.38 $\pm$ 0.073	-	MS, RI
19	<i>cis</i> -Chrysanthenol	1136	0.26 $\pm$ 0.032	-	MS, RI
20	Borneol	1150	2.54 $\pm$ 0.044	2.14 $\pm$ 0.032	MS, RI
21	<i>p</i> -Menth-1-en-4-ol	1163	1.51 $\pm$ 0.077	0.59 $\pm$ 0.036	MS, RI
22	$\alpha$ -Terpineol	1174	-	1.12 $\pm$ 0.032	MS, RI
23	$\beta$ -Citral	1174	5.5 $\pm$ 0.081	-	MS, RI
24	Estragole	1178	0.68 $\pm$ 0.008	0.2 $\pm$ 0.032	MS, RI
25	Neral	1218	1.09 $\pm$ 0.118	0.55 $\pm$ 0.040	MS, RI
26	Geraniol	1228	0.59 $\pm$ 0.032	-	MS, RI
27	$\alpha$ -Citral	1247	1.18 $\pm$ 0.016	0.35 $\pm$ 0.040	MS, RI
28	Anethole	1263	-	0.24 $\pm$ 0.024	MS, RI
29	Bornyl acetate	1273	-	0.3 $\pm$ 0.040	MS, RI
30	2-Undecanone	1280	0.53 $\pm$ 0.024	1.12 $\pm$ 0.097	MS, RI
31	Citronellol acetate	1302	-	0.68 $\pm$ 0.016	MS, RI
32	Eugenol	1331	-	0.5 $\pm$ 0.040	MS, RI
33	Nerol acetate	1352	-	0.4 $\pm$ 0.048	MS, RI
34	Cyclosativene	1367	-	0.57 $\pm$ 0.016	MS, RI
35	$\alpha$ -Copaene	1376	0.46 $\pm$ 0.032	0.85 $\pm$ 0.048	MS, RI
36	Aromadendrene	1386	1.63 $\pm$ 0.024	-	MS, RI
37	$\beta$ -elemene	1388	-	0.51 $\pm$ 0.040	MS, RI
38	7-epi-Sesquithujene	1404	-	0.34 $\pm$ 0.032	MS, RI
39	$\beta$ -Caryophyllene	1416	0.29 $\pm$ 0.040	0.94 $\pm$ 0.040	MS, RI
40	Sesquisabinene	1446	0.67 $\pm$ 0.057	-	MS, RI
41	Longifolene	1447	-	0.5 $\pm$ 0.016	MS, RI
42	$\alpha$ -Curcumene	1475	14.23 $\pm$ 0.065	28.19 $\pm$ 0.028	MS, RI
43	Eudesma-4(14),11-diene	1481	1.37 $\pm$ 0.016	2 $\pm$ 0.089	MS, RI
44	Zingiberene	1491	7.9 $\pm$ 0.040	14.84 $\pm$ 0.048	MS, RI
45	$\gamma$ -Cadinene	1494	1.92 $\pm$ 0.024	5.05 $\pm$ 0.040	MS, RI
46	$\beta$ -Bisabolene	1505	8.03 $\pm$ 0.032	11.68 $\pm$ 0.097	MS, RI
47	$\alpha$ -Selinene	1513	0.38 $\pm$ 0.016	1.21 $\pm$ 0.008	MS, RI



Table 1. Cont.

<sup>a</sup> Compound	<sup>b</sup> Retention Index (RI)	Fresh Ginger	Dry Ginger	Identification
48 $\beta$ -Sesquiphellandrene	1519	7.87 $\pm$ 0.024	15.06 $\pm$ 0.297	MS, RI
49 7-epi-cis-sesquisabinene hydrate	1523	1.35 $\pm$ 0.040	-	MS, RI
50 $\alpha$ -trans-Bergamotene	1526	-	0.57 $\pm$ 0.028	MS, RI
51 Globulol	1530	0.68 $\pm$ 0.008	-	MS, RI
52 Selina-3,7(11)-diene	1538	-	0.43 $\pm$ 0.016	MS, RI
53 $\beta$ -Oplopenone	1540	0.4 $\pm$ 0.016	-	MS, RI
54 <i>trans</i> -Nerolidol	1550	1.95 $\pm$ 0.028	0.76 $\pm$ 0.032	MS, RI
55 Zingiberenol	1591	3.75 $\pm$ 0.040	-	MS, RI
56 Agarospirol	1598	0.56 $\pm$ 0.032	-	MS, RI
57 Eudesm-4(14)-en-11-ol	1631	0.36 $\pm$ 0.016	0.3 $\pm$ 0.024	MS, RI
58 Viridiflorol	1637	-	0.38 $\pm$ 0.048	MS, RI
59 Ishwarol B	1674	1 $\pm$ 0.163	0.95 $\pm$ 0.040	MS, RI
60 Nerolidyl acetate	1754	-	0.98 $\pm$ 0.016	MS, RI
61 Humulenol	1762	0.58 $\pm$ 0.024	-	MS, RI
62 Corymbolone	1785	0.78 $\pm$ 0.016	-	MS, RI
63 Geranyl-p-cymene	1937	0.37 $\pm$ 0.028	0.22 $\pm$ 0.016	MS, RI
64 geranyl- $\alpha$ -terpinene	1962	0.33 $\pm$ 0.028	-	MS, RI
65 1-Heptatriacotanol	3942	0.98 $\pm$ 0.024	-	MS, RI
<b>No. of identified compounds</b>		<b>45</b>	<b>43</b>	
<b>Monoterpene hydrocarbons %</b>		11.17	1.14	
<b>Oxygenated monoterpenes %</b>		25.26	9.8	
<b>Sesquiterpene hydrocarbons %</b>		44.75	82.87	
<b>Oxygenated sesquiterpenes %</b>		11.41	2.96	
<b>Miscellaneous %</b>		5.03	3.72	
<b>Total percentage identified</b>		<b>97.62</b>	<b>99.82</b>	

<sup>a</sup> The compounds are listed according to elution order. <sup>b</sup> Retention index (RI) calculated on Rtx-5MS fused bonded column. MS, mass spectral. The major components are bold-highlighted.

### 3.2. Effect of Sun Drying on the Total Phenolic Content (TPC), Total Flavonoid Content (TFC) and Antiviral Activity of Ginger Extracts

Drying treatment showed a varying effect on the TPC and TFC of ginger samples. As demonstrated in Table 2, the TPC in fresh ginger was  $39.33 \pm 2.57 \mu\text{g}$  of GAE/mg, which is close to the report of [42], who found the TPC of ginger to be  $24.63 \pm 0.43 \text{ mg}$  GAE/g. Other studies reported different results, as in [43]. These differences could be attributed to several factors such as varieties, genetics, and regions of cultivation of ginger. However, the TPC of dried ginger decreased considerably compared to fresh ginger. This could be attributed to prolonged drying time, which could cause the initiation of oxidative enzymes such as peroxidase and polyphenol oxidase through the drying procedure leading to the loss of phenolic groups. Moreover, variations in the chemical structure of phenols, as in the bindings of phenols to proteins, might also cause a loss of phenolic content, as mentioned in previous studies [44].

Table 2. Changes of TPC, TFC, and antiviral activity of ginger extracts.

	Fresh Ginger	Dry Ginger
Total phenolic content ( $\mu\text{g}$ of GAE/mg)	39.33 $\pm$ 2.5	20.96 $\pm$ 1.2
Total flavonoid content ( $\mu\text{g}$ rutin eq/mg)	11.56 $\pm$ 1.2	1.34 $\pm$ 0.9
Antiviral activity (IC <sub>50</sub> )	28.5 $\pm$ 0.8	20.56 $\pm$ 0.4

In terms of TFC, it is worth noting that sun-dried samples showed low TFC  $1.34 \pm 0.9 \mu\text{g}$  RE/mg than fresh samples. Since flavonoids are thermolabile compounds as previously mentioned [45], sun drying caused a loss of TFC, verifying that the duration and

temperature of drying could trigger the loss of such macromolecules. Previous studies also showed that drying significantly decreased the TFC of several herbs such as sage, thyme and guava [46,47].

The current study assessed the antiviral activity of fresh and dry ginger extracts using crystal violet assay. According to Table S1, the tested samples showed moderate antiviral activity against 229 E (low-pathogenic coronavirus). Earlier studies provide evidence regarding the potential effects of ginger against SARS-CoV-2 infection especially due to its antiviral, anti-inflammatory, antioxidative, and immunomodulatory effects [48].

### 3.3. Absorption, Distribution, Metabolism, Excretion, and Toxicity (ADMET) and Pharmacokinetic Studies

Using pkCSM (a Cambridge online source, link: <http://bleoberis.bioc.cam.ac.uk/pkcsm/prediction>, accessed on 15 May 2022), the ADMET and pharmacokinetic properties of the compounds were checked to ensure that the molecules exhibited the potential of a drug and were validated by MedChemDesigner™ software, version 3.0 [49], which predicted the values with great accuracy. The expected values for the compounds (1N1–1N9) show that the molecules have a great solubility potential, both in water,  $-5.96$  to  $2.63$  (log mol/L), and  $\text{CaCO}_2$  permeability of  $1.54$  to  $1.25$  (log Papp in 10 cm/s). Intrinsic water solubility and solubility at pH 7.4 (LogS) were found in the range of  $-5.45$  to  $-2.00$ . Intestinal absorption (human) was  $\approx 95$  (% absorbed) and skin permeability was  $-2.42$  to  $-1.27$ , (log Kp). Blood–brain barrier (BBB) permeability was  $0.58$  to  $0.80$  (log BB) and CNS permeability was  $-2.21$  to  $-1.51$  (log PS). The value of clearance, which is the pharmacokinetic parameter that represents the rate of drug elimination divided by its plasma concentration, was quite favorable for all the molecules ( $1.01$  to  $1.51$  log mL/min/kg) and implies that the molecule would not accumulate in the body and hence is non-toxic and non-hepatotoxic. Oral rat acute toxicity ( $\text{LD}_{50}$ ) was found to be in the range of  $1.49$  to  $1.92$  mol/kg, and oral rat chronic toxicity (LOAEL) was  $1.32$  to  $2.31$  (log mg/kg/bw/day) with a maximum tolerated dose (human) in the range of  $0.24$  to  $0.96$  log mg/kg/day. These results reveal that the molecules possess good ADMET properties, which are required for a molecule to show drug-like properties.

From the predicted pharmacokinetic parameters and after applying Lipinski's filters as in Table 3, it appears that the molecules under study show good drug-likeness properties and therefore could be considered good drug candidates for further studies.

**Table 3.** Lipinski's filters for drug-likeness.

Compound	M.Wt	LogP *	LogD #	<sup>a</sup> HBA	HBD	RBs	Ro5 (Y/N)
4-Thujanol (1N1)	154.14	1.69	1.89	1	1	1	Y
Neral (1N2)	152.12	2.16	2.66	1	0	4	Y
Geranial (1N3)	152.12	2.16	2.66	1	0	4	Y
Camphene (1N4)	136.13	2.84	2.86	0	0	0	Y
$\alpha$ -Curcumene (1N5)	202.34	5.19	5.39	0	0	4	Y
Zingiberene (1N6)	204.19	4.55	4.87	0	0	4	Y
$\gamma$ -Cadinene (1N7)	204.19	4.22	4.51	0	0	1	Y
$\beta$ -Bisabolene (1N8)	204.19	4.41	4.88	0	0	4	Y
$\beta$ -sesquiphellandrene (1N9)	204.19	4.59	4.92	0	0	4	Y
<sup>†</sup> Chloroquine	320.89	3.39	0.40	1	2	8	Y
<sup>†</sup> Favipiravir	157.10	$-1.19$	0.25	3	2	1	Y

\* At PH 7.4; # calculated using ChemAxonLogD predictor; <sup>†</sup> Taken from referred sources; <sup>a</sup> HBA—hydrogen bond acceptor, HBD—hydrogen bond donor, obtained by Marvin Sketch 22.11; RB: Rotatable bonds; Ro5 (Y/N): rule of five followed or not; Y: Yes; N: No.

The bioavailability radar of the molecules obtained from Swiss ADME displayed some of the molecules exhibiting promising physicochemical properties for oral bioavailability. The ideal spaces of six physicochemical parameters—for example, polarity, size, solubility, lipophilicity, flexibility, and saturation for oral bioavailability of the representative

molecules 1N5, 1N6, 1N8, and 1N9—are within the pink-colored area of Figure 1 [50,51]. If the radar plot of a molecule falls entirely in the pink area, it is considered drug-like. The optimal range for each property is represented by the pink area (lipophilicity: XLOGP3 between  $-0.7$  and  $+5.0$ , size: MW between 150 and 500 g/mol, polarity: TPSA between 20 and  $130 \text{ \AA}^2$ , solubility: log S not higher than 6, saturation: fraction of carbons in the  $sp^3$  hybridization not less than 0.25, and flexibility: no more than nine rotatable bonds).

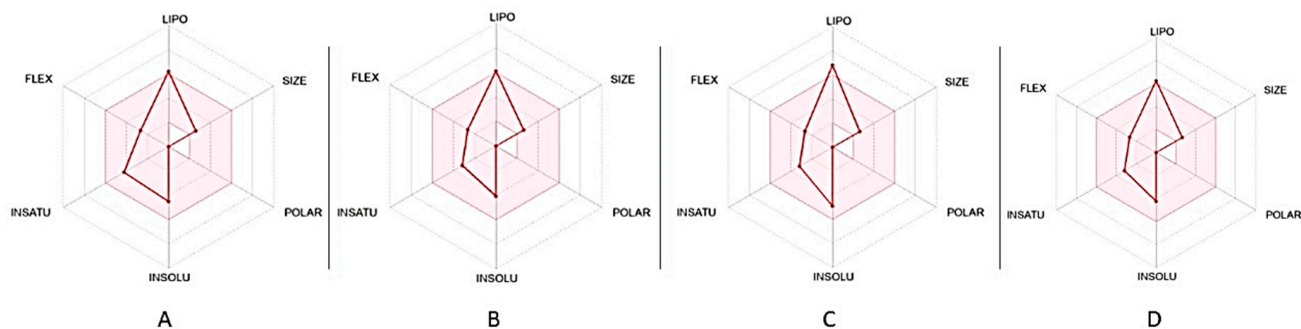


**Figure 1.** Bioavailability radar plot of the most active constituents: (A) 1N5, (B) 1N6, (C) 1N8, and (D) 1N9. POLAR (polarity), LIPO (lipophilicity), INSOLU (solubility), FLEX (flexibility), and INSATU (saturation).

Although efficacy and toxicity are responsible for the failure of many drug development projects, poor pharmacokinetic properties and low bioavailability are major hurdles. The two pharmacokinetic conducts, gastrointestinal absorption and brain access, are crucial to estimate at various drug discovery stages. BOILED-Egg (Brain Or Intestinal Estimated permeation method) is proposed to be an accurate predictive model that works by computing the lipophilicity and polarity of small molecules and is therefore considered of great importance in lead optimization. Passive gastrointestinal absorption (HIA) and brain access (BBB) are the two key ADME parameters that could be predicted simultaneously by the BOILED-Egg model [52]. This model is conceptually simple, relying only on two physicochemical descriptors (WLOGP and TPSA) for lipophilicity and apparent polarity. It has been built with extreme care regarding statistical significance and robustness [52]. As shown in Figure S4, this egg-shaped plot includes the yolk (i.e., the physicochemical space for highly probable BBB permeation) and the white (i.e., the physicochemical space for highly probable HIA absorption). The outer grey region represents the molecules that are predicted to show low absorption and limited brain penetration. The BOILED-Egg model has been of great importance as a model for the interpretation and efficient translation of molecular design in a variety of drug discovery settings. The representative molecules under study, particularly 1N9, as shown in Figure S4, are predicted to be well-absorbed without any possible access to the brain (in the white) and PGP- (red dot).

### 3.4. In Silico Molecular Docking

The compounds were subjected to molecular docking experiments to validate the expected target. The molecules' 2D structures were transformed to energy-minimized 3D structures and employed for docking. The 3C-Like proteinase ( $3CL^{Pro}$ ) of the severe acute respiratory syndrome coronavirus 2 (SARS-CoV-2) is an important drug target due to its vital role in viral replication. The discovery of the X-ray crystal structure of  $3CL^{Pro}$  has been greatly useful in searching for potential lead molecules that could bind the target and emerge as potential drug candidates for further development. Focusing on the main proteases ( $3CL^{Pro}/M^{Pro}$ ), with PDB ID 6LU7, docking of the main components (1N1-1N9) was performed to identify the lead molecules. MOE 2015.10 was used to carry out the molecular docking calculations, and the conformation with the lowest binding free energy was used for analysis. Docking studies revealed that the lead molecules bind very well with the target with low binding energy values, which was attributed to the interaction of the



molecules with the amino acid residues within the active site pocket of the target protein. It can be seen that the molecules bind very well within the active site pocket and show different types of interactions with the amino acid residues in the two-dimensional images of Figure 2. Docking results revealed that the most active components were 1N5, 1N6, 1N8, and 1N9, compared to the other components based on the energy score and interaction with the target protein. All the active components displayed a docking score  $>8.963$ , which is higher than the energy score given by chloroquine ( $-6.293$  Kcal/mol), hydroxychloroquine ( $-5.573$  Kcal/mol), and favipiravir ( $-4.233$  Kcal/mol). The lead molecules and the other derivatives also showed good ADMET properties and passed Lipinski's filters for drug-likeness. Collectively, these results could pave the way for the development of plant-based small molecules as an effective treatment regimen against COVID-19.

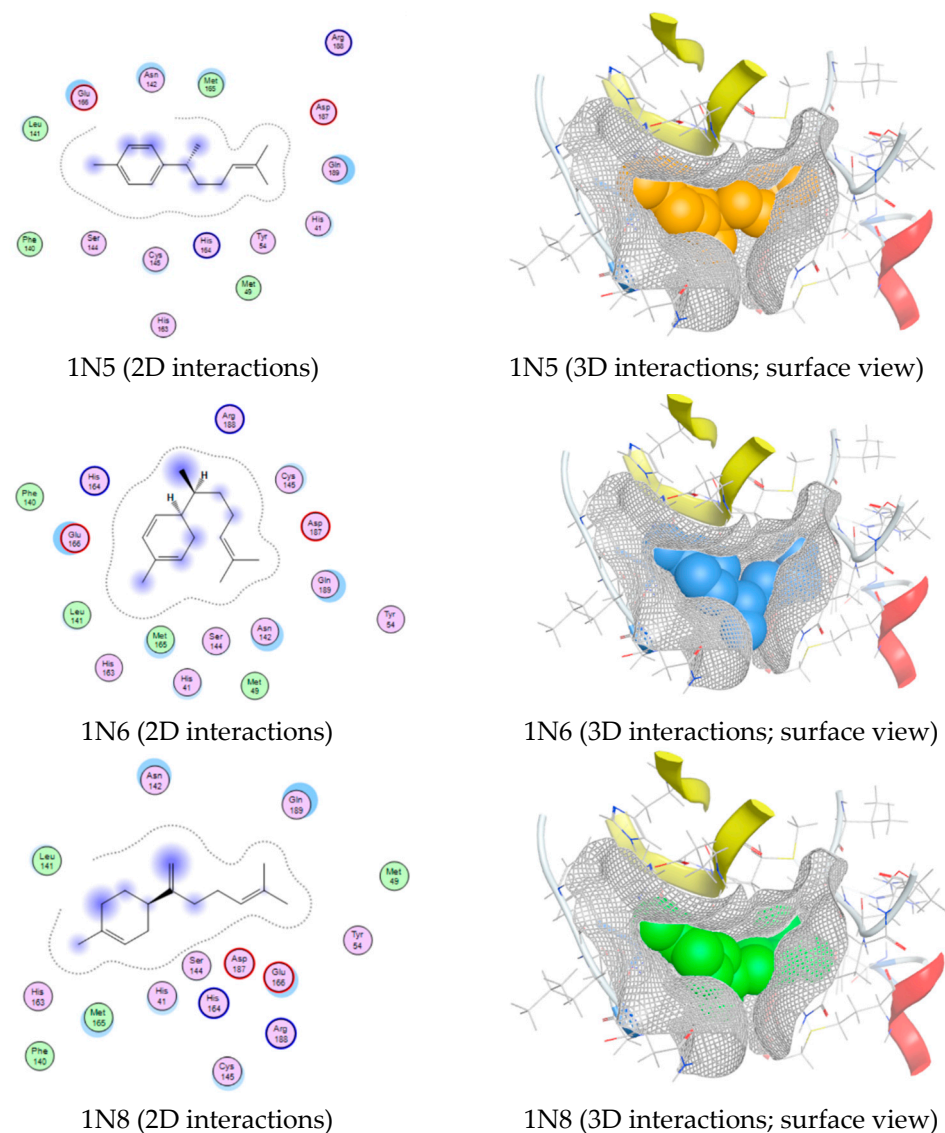
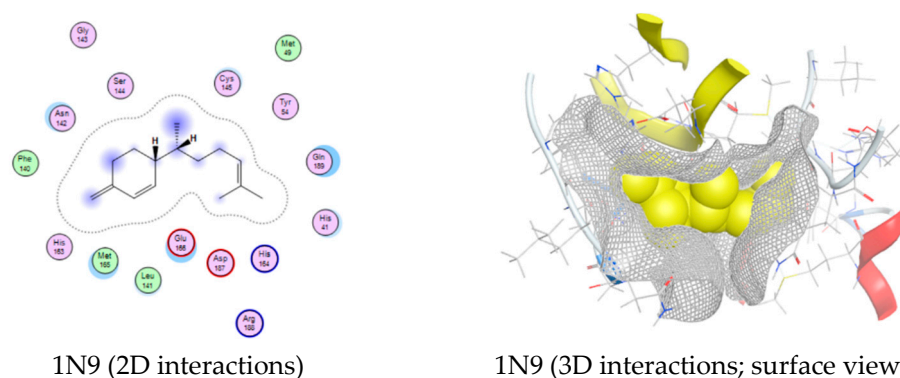


Figure 1. Cont.



**Figure 2.** Docked images of the most active molecules. Ligand interactions within the active site pocket of the protein 6LU7, shown as 2D and 3D interactions; surface view inside the active site pocket.

Viruses that infect humans are known to encode one or more proteases that are crucial in the viral life cycle. Proteases cleave the viral polyprotein, helping continue the viral replication process, and are ideal drug targets [53]. The SARS-CoV-2 replicase enzyme encodes two polyproteins, pp1a and pp1ab, that produce all the functional polypeptide units responsible for the replication and transcription of the virus. The catalytic cleavage activity of 3CLPro at various subsites of the polypeptide results in the release of the polypeptides. This cleavage process is known to be conserved in the 3CLPro of all the coronaviruses [54], which is believed to play a vital role in viral replication. Interestingly, due to the absence of any close homolog in humans, this protease has been regarded as a promising therapeutic target for COVID-19 treatment [55].

### 3.5. Chemometric Analysis

Principal component analysis (PCA) was applied to segregate fresh and dry ginger samples and recognize any significant association between them. A matrix of the total number of samples and their replicates (six samples) multiplied by 65 variables (GC-MS peak area %) was constructed in MS Excel<sup>®</sup>, then subjected to chemometric analysis (PCA). The PCA score plot accounting for 100% of the variation in the dataset of Figure 3a highlights that the first principal component (100%) completely discriminates dry ginger (DG) (positive PC1 values) from fresh ginger (FG) (negative PC1). Figure 3b displays the loading plot with the main volatile constituents responsible for the segregation between fresh and dry ginger, where  $\alpha$ -curcumene and 4-thujanol were the main markers responsible for the discrimination between dry and fresh ginger, respectively.

Moreover, partial least-squares (PLS) was applied to find a correlation between the volatile constituents and their antiviral activity. The PLS-R model was constructed by the data matrix X, containing the peak area of the GC/MS, and the response y vectors, containing the antiviral activity data, respectively. The model performance was estimated by the parameters of root mean square error of calibration (RMSEC), root mean square error of validation (RMSEV), and correlation ( $R^2$ ). PLS-R1 model parameters, including slope, offset, RMSEC, RMSEV, and  $R^2$ , are shown in Table 4, indicating a strong prediction ability of the PLS regression model. PLS-R1 models showed excellent linearity and accuracy with  $R^2 > 0.98$ , a slope close to 1 (a value close to 1 means the predicted values are close to the reference), low differences between RMSEC and root, and mean square error of validation (RMSEV) reveal the robustness of the model. The prediction performance for the developed models is shown in Table S2. The results displayed that the antiviral activity is correctly predicted with  $\pm 5\%$  accuracy.

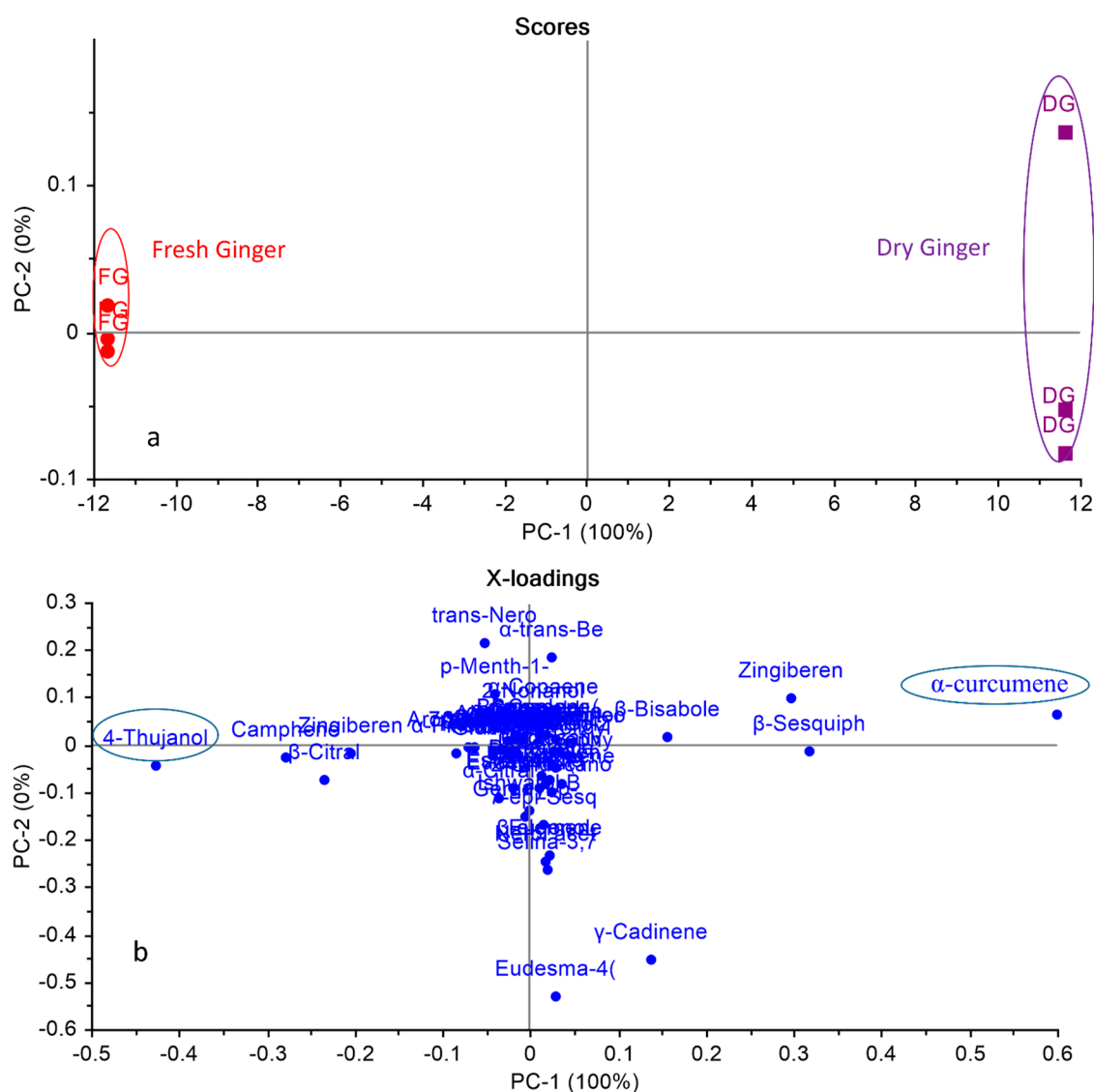


Figure 3. PCA score plot (a) and loading plot (b) based on GC-MS chemical profile of the volatile oils of fresh ginger (FG) and dry ginger (DG).

Table 4. PLS-R model parameters used for prediction.

Antiviral Activity	Data Type	Slope	Offset	PLS-R	
				RMSE	R <sup>2</sup>
	Cal.	0.9923	0.1876	0.3489	0.9923
	Val.	0.9884	0.2818	0.5232	0.9880

R<sup>2</sup>: Correlation, Cal. Calibration, Val. Validation.

#### 4. Conclusions

It can be concluded from this study that sun drying affects the composition and yield of bioactive compounds where the drying process increased  $\alpha$ -curcumene  $\beta$ -sesquiphellandrene and zingiberine percentage. Generally, the percentage of sesquiterpene hydrocarbons increased after drying, with a decrease in oxygenated mono- and sesquiterpene hydrocarbons and the conversion of some monoterpene alcohols to their corresponding acetates. Additionally, the results emphasized that dried ginger decreased the flavonoid and total phenolic content. Antiviral activity increased after drying and was supported by in silico molecular docking. Thus, ginger is rich in valuable phytoconstituents which showed promising therapy in viral infections such as COVID-19.

**Supplementary Materials:** The following supporting information can be downloaded at: <https://www.mdpi.com/article/10.3390/agronomy12112763/s1>. Figure S1: Standard calibration curve of gallic acid; Figure S2: Standard calibration curve of rutin; Figure S3: GC/MS chromatogram for fresh ginger volatile oil (a); 1 camphene, 2 4-Thujanol, 3 Borneol, 4  $\beta$ -Citral, 5  $\alpha$ -Curcumene, 6 Zingiberene and 7  $\beta$ -Bisabolene; dry ginger volatile oil (b); 1  $\alpha$ -Curcumene, 2 Zingiberene, 3  $\beta$ -Bisabolene and 4  $\beta$ -Sesquiphellandrene; Figure S4: BOILED Egg predictive model for one of the most active components (1N9). All the active components displayed similar properties; Table S1: Selectivity index of fresh and dry ginger extracts; Table S2: Results of calibration and predictive ability of the PLS-R model.

**Author Contributions:** Data curation, Y.A.E., M.Y.W., H.A.G. and N.K.; conceptualization, Y.A.E., M.Y.W., H.A.G. and N.K.; formal analysis, Y.A.E. and N.K.; investigation, Y.A.E. and N.K.; methodology, Y.A.E., M.Y.W., H.A.G. and N.K.; project administration, Y.A.E. and N.K.; resources, Y.A.E. and N.K.; supervision, Y.A.E. and N.K.; validation, Y.A.E. and N.K.; visualization, Y.A.E. and N.K.; writing—original draft preparation and editing, Y.A.E., M.Y.W., H.A.G. and N.K.; reviewing, Y.A.E., M.Y.W., H.A.G., M.O.L., R.M.K. and N.K.; software, M.Y.W. and H.A.G.; funding, M.O.L. and R.M.K. All authors have read and agreed to the published version of the manuscript.

**Funding:** This research was funded by the Deanship of Scientific Research (DSR) at King Abdulaziz University (KAU), Jeddah, Saudi Arabia, under grant number (RG-27-166-43).

**Acknowledgments:** The Deanship of Scientific Research (DSR) at King Abdulaziz University (KAU), Jeddah, Saudi Arabia, has funded this project under grant no. (RG-27-166-43). Therefore, all the authors acknowledge, with thanks, the DSR for technical and financial support.

**Conflicts of Interest:** The authors declare no conflict of interest.

## References

1. Ali, B.H.; Blunden, G.; Tanira, M.O.; Nemmar, A. Some phytochemical, pharmacological and toxicological properties of ginger (*Zingiber officinale* Roscoe): A review of recent research. *Food Chem. Toxicol.* **2008**, *46*, 409–420. [[CrossRef](#)] [[PubMed](#)]
2. Muntean, D.; Licker, M.; Alexa, E.; Popescu, I.; Jianu, C.; Buda, V.; Dehelean, C.A.; Ghiulai, R.; Horhat, F.; Horhat, D.; et al. Evaluation of essential oil obtained from *Mentha × piperita* L. against multidrug-resistant strains. *Infect. Drug Resist.* **2019**, *12*, 2905. [[CrossRef](#)] [[PubMed](#)]
3. Bakkali, F.; Averbeck, S.; Averbeck, D.; Idaomar, M. Biological effects of essential oils—A review. *Food Chem. Toxicol.* **2008**, *46*, 446–475. [[CrossRef](#)] [[PubMed](#)]
4. Ashmawy, A.; Mostafa, N.; Eldahshan, O. GC/MS Analysis and Molecular Profiling of Lemon Volatile Oil against Breast Cancer. *J. Essent. Oil Bear. Plants* **2019**, *22*, 903–916. [[CrossRef](#)]
5. Kalemba, D.; Kunicka, A. Antibacterial and antifungal properties of essential oils. *Curr. Med. Chem.* **2003**, *10*, 813–829. [[CrossRef](#)] [[PubMed](#)]
6. Dorman, H.D.; Koşar, M.; Kahlos, K.; Holm, Y.; Hiltunen, R. Antioxidant properties and composition of aqueous extracts from *Mentha* species, hybrids, varieties, and cultivars. *J. Agric. Food Chem.* **2003**, *51*, 4563–4569. [[CrossRef](#)]
7. Bhagat, M.; Sangral, M.; Arya, K.; Rather, R.A. Chemical characterization, biological assessment and molecular docking studies of essential oil of *Ocimum viride* for potential antimicrobial and anticancer activities. *BioRxiv* **2018**, 390906. [[CrossRef](#)]
8. Seo, S.; Fang, F.; Kang, I. Ginger (*Zingiber officinale*) attenuates obesity and adipose tissue remodeling in high-fat diet-fed c57bl/6 mice. *Int. J. Environ. Res. Public Health* **2021**, *18*, 631. [[CrossRef](#)]
9. Mošovská, S.; Nováková, D.; Kaliňák, M. Antioxidant activity of ginger extract and identification of its active components. *Acta Chim. Slovaca* **2015**, *8*, 115–119. [[CrossRef](#)]
10. Famurewa, A.V.; Emuekele, P.O.; Jaiyeoba, K.F. Effect of drying and size reduction on the chemical and volatile oil contents of ginger (*Zingiber officinale*). *J. Med. Plants Res.* **2011**, *5*, 2941–2944.
11. Doymaz, İ. Air-drying characteristics of tomatoes. *J. Food Eng.* **2007**, *78*, 1291–1297. [[CrossRef](#)]
12. Deshmukh, A.W.; Varma, M.N.; Yoo, C.K.; Wasewar, K.L. Investigation of Solar Drying of Ginger (*Zingiber officinale*): Empirical Modelling, Drying Characteristics, and Quality Study. *Chin. J. Eng.* **2014**, *2014*, 305823. [[CrossRef](#)]
13. An, K.; Zhao, D.; Wang, Z.; Wu, J.; Xu, Y.; Xiao, G. Comparison of different drying methods on Chinese ginger (*Zingiber officinale* Roscoe): Changes in volatiles, chemical profile, antioxidant properties, and microstructure. *Food Chem.* **2016**, *197*, 1292–1300. [[CrossRef](#)] [[PubMed](#)]
14. Islam, M.T.; Sarkar, C.; El-Kersh, D.M.; Jamaddar, S.; Uddin, S.J.; Shilpi, J.A.; Mubarak, M.S. Natural products and their derivatives against coronavirus: A review of the non-clinical and pre-clinical data. *Phytother. Res.* **2020**, *34*, 2471–2492. [[CrossRef](#)]
15. Rasool, A.; Khan, M.-U.; Ali, M.A.; Anjum, A.A.; Ahmed, I.; Aslam, A.; Mustafa, G.; Masood, S.; Ali, M.A.; Nawaz, M. Anti-Avian influenza virus H9N2 activity of aqueous extracts of *Zingiber officinalis* (Ginger) & *Allium sativum* (Garlic) in chick embryos. *Pak. J. Pharm. Sci.* **2017**, *30*, 1341–1344.



16. Mao, Q.-Q.; Xu, X.-Y.; Cao, S.-Y.; Gan, R.-Y.; Corke, H.; Beta, T.; Li, H.-B. Bioactive Compounds and Bioactivities of Ginger (*Zingiber officinale* Roscoe). *Foods* **2019**, *8*, 185. [[CrossRef](#)]
17. Cheng, V.C.C.; Lau, S.K.P.; Woo, P.C.Y.; Yuen, K.-Y. Severe acute respiratory syndrome coronavirus as an agent of emerging and reemerging infection. *Clin. Microbiol. Rev.* **2007**, *20*, 660–694. [[CrossRef](#)]
18. Lee, N.; Hui, D.; Wu, A.; Chan, P.; Cameron, P.; Joynt, G.M.; Ahuja, A.; Yung, M.Y.; Leung, C.; To, K.; et al. A major outbreak of severe acute respiratory syndrome in Hong Kong. *N. Engl. J. Med.* **2003**, *348*, 1986–1994. [[CrossRef](#)]
19. Wang, L.; Wang, Y.; Ye, D.; Liu, Q. Review of the 2019 novel coronavirus (SARS-CoV-2) based on current evidence. *Int. J. Antimicrob. Agents* **2020**, *55*, 105948. [[CrossRef](#)]
20. Zhu, N.; Zhang, D.; Wang, W.; Li, X.; Yang, B.; Song, J.; Zhao, X.; Huang, B.; Shi, W.; Lu, R.; et al. A Novel Coronavirus from Patients with Pneumonia in China, 2019. *N. Engl. J. Med.* **2020**, *382*, 727–733. [[CrossRef](#)]
21. Huang, D.; Lian, X.; Song, F.; Ma, H.; Lian, Z.; Liang, Y.; Qin, T.; Chen, W.; Wang, S. Clinical features of severe patients infected with 2019 novel coronavirus: A systematic review and meta-analysis. *Ann. Transl. Med.* **2020**, *8*, 576. [[CrossRef](#)] [[PubMed](#)]
22. Chen, Y.; Liu, Q.; Guo, D. Emerging coronaviruses: Genome structure, replication, and pathogenesis. *J. Med. Virol.* **2020**, *92*, 418–423. [[CrossRef](#)] [[PubMed](#)]
23. Paul, E.; Steptoe, A.; Fancourt, D. Attitudes towards vaccines and intention to vaccinate against COVID-19: Implications for public health communications. *Lancet Reg. Health Eur.* **2021**, *1*, 100012. [[CrossRef](#)] [[PubMed](#)]
24. Cvjetkovic, S.J.; Jeremic, V.L.; Tiosavljevic, D.V. Knowledge and attitudes toward vaccination: A survey of Serbian students. *J. Infect. Public Health* **2017**, *10*, 649–656. [[CrossRef](#)]
25. Veeresham, C. Natural products derived from plants as a source of drugs. *J. Adv. Pharm. Technol. Res.* **2012**, *3*, 200–201. [[CrossRef](#)]
26. Panyod, S.; Ho, C.-T.; Sheen, L.-Y. Dietary therapy and herbal medicine for COVID-19 prevention: A review and perspective. *J. Tradit. Complement. Med.* **2020**, *30*, 420–427. [[CrossRef](#)] [[PubMed](#)]
27. Yang, Y.; Islam, M.S.; Wang, J.; Li, Y.; Chen, X. Traditional Chinese medicine in the treatment of patients infected with 2019-New Coronavirus (SARS-CoV-2): A review and perspective. *Int. J. Biol. Sci.* **2020**, *16*, 1708–1717. [[CrossRef](#)]
28. Bachir, B.; Atanasio, P. Medicinal Plants as Sources of Active Molecules Against COVID-19. *Front. Pharmacol.* **2020**, *11*, 1189.
29. Llivisaca-Contreras, S.A.; Naranjo-Morán, J.; Pino-Acosta, A.; Pieters, L.; Vanden Berghe, W.; Manzano, P.; Vargas-Pérez, J.; León-Tamariz, F.; Cevallos, J.M. Plants and Natural Products with Activity against Various Types of Coronaviruses: A Review with Focus on SARS-CoV-2. *Molecules* **2021**, *26*, 4099. [[CrossRef](#)]
30. Mostafa, N. Antibacterial Activity of Ginger (*Zingiber officinale*) Leaves Essential Oil Nanoemulsion against the Cariogenic *Streptococcus mutans*. *J. Appl. Pharm. Sci.* **2018**, *8*, 34–41.
31. Attard, E. A rapid microtitre plate Folin-Ciocalteu method for the assessment of polyphenols. *Open Life Sci.* **2013**, *8*, 48–53. [[CrossRef](#)]
32. Kiranmai, M.; Kumar, C.B.; Ibrahim, M. Comparison of total flavanoid content of *Azadirachta indica* root bark extracts prepared by different methods of extraction. *Res. J. Pharm. Biol. Chem. Sci.* **2011**, *2*, 254–261.
33. Donalisio, M. In vitro anti-Herpes simplex virus activity of crude extract of the roots of *Nauclea latifolia* Smith (Rubiaceae). *BMC Complement. Altern. Med.* **2013**, *13*, 266. [[CrossRef](#)] [[PubMed](#)]
34. Pauwels, R.; Balzarini, J.; Baba, M.; Snoeck, R.; Schols, D.; Herdewijn, P.; Desmyter, J.; De Clercq, E. Rapid and automated tetrazolium-based colorimetric assay for the detection of anti-HIV compounds. *J. Virol. Methods* **1988**, *20*, 309–321. [[CrossRef](#)]
35. Singab, A.N.B.; Mostafa, N.M.; Elkhawas, Y.A.; Al-Sayed, E.; Bishr, M.M.; Elissawy, A.M.; Elnaggar, M.S.; Fawzy, I.M.; Salama, O.M.; Tsai, Y.-H.; et al. Cyclodipeptides: Isolation from Endophytic Fungi of *Sarcophyton ehrenbergi* and Verification of Their Larvicidal Activity via In-Vitro and In-Silico Studies. *Mar. Drugs* **2022**, *20*, 331. [[CrossRef](#)]
36. Meanwell, N.A. Improving Drug Candidates by Design: A Focus on Physicochemical Properties As a Means of Improving Compound Disposition and Safety. *Chem. Res. Toxicol.* **2011**, *24*, 1420–1456. [[CrossRef](#)] [[PubMed](#)]
37. Kearns, E.H.; Di, L. *Drug-Like Properties: Concepts, Structure Design and Methods*; Elsevier: New York, NY, USA, 2008.
38. Gleeson, M.P. Generation of a Set of Simple, Interpretable ADMET Rules of Thumb. *J. Med. Chem.* **2008**, *51*, 817–834. [[CrossRef](#)]
39. Alrasheid, A.A.; Babiker, M.Y.; Awad, T.A. Evaluation of certain medicinal plants compounds as new potential inhibitors of novel corona virus (COVID-19) using molecular docking analysis. *Silico Pharmacol.* **2021**, *9*, 10. [[CrossRef](#)]
40. Huang, B.; Wang, G.; Chu, Z.; Qin, L. Effect of oven drying, microwave drying, and silica gel drying methods on the volatile components of ginger (*Zingiber officinale* Roscoe) by HS-SPME-GC-MS. *Dry. Technol.* **2012**, *30*, 248–255. [[CrossRef](#)]
41. Ding, S.; An, K.; Zhao, C.; Li, Y.; Guo, Y.; Wang, Z. Effect of drying methods on volatiles of Chinese ginger (*Zingiber officinale* Roscoe). *Food Bioprod. Process.* **2012**, *90*, 515–524. [[CrossRef](#)]
42. Puengphian, C.; Sirichote, A. [6]-Gingerol content and bioactive properties of ginger (*Zingiber officinale* Roscoe) extracts from supercritical CO<sub>2</sub> extraction. *Asian J. Food Agro-Ind.* **2008**, *1*, 29–36.
43. Gümüşay, Ö.A.; Borazan, A.A.; Ercal, N.; Demirkol, O. Drying effects on the antioxidant properties of tomatoes and ginger. *Food Chem.* **2015**, *173*, 156–162. [[CrossRef](#)] [[PubMed](#)]
44. Toor, R.K.; Savage, G.P. Effect of semi-drying on the antioxidant components of tomatoes. *Food Chem.* **2006**, *94*, 90–97. [[CrossRef](#)]
45. Zheng, G.; Chao, Y.; Liu, M.; Yang, Y.; Zhang, D.; Wang, K.; Tao, Y.; Zhang, J.; Li, Y.; Wei, M. Evaluation of dynamic changes in the bioactive components in Citri Reticulatae Pericarpium (*Citrus reticulata* ‘Chachi’) under different harvesting and drying conditions. *J. Sci. Food Agric.* **2021**, *101*, 3280–3289. [[CrossRef](#)]



46. Nunes, J.C.; Lago, M.G.; Castelo-Branco, V.N.; Oliveira, F.R.; Torres, A.G.; Perrone, D.; Monteiro, M. Effect of drying method on volatile compounds, phenolic profile and antioxidant capacity of guava powders. *Food Chem.* **2016**, *197*, 881–890. [[CrossRef](#)]
47. Rababah, T.M.; Alhamad, M.; Al-Mahasneh, M.; Ereifej, K.; Andrade, J.; Altarifi, B.; Almajwal, A.; Yang, W. Effects of drying process on total phenolics, antioxidant activity and flavonoid contents of common mediterranean herbs. *Int. J. Agric. Biol. Eng.* **2015**, *8*, 145–150.
48. Jafarzadeh, A.; Jafarzadeh, S.; Nemati, M. Therapeutic potential of ginger against COVID-19: Is there enough evidence? *J. Tradit. Chin. Med. Sci.* **2021**, *8*, 267–279. [[CrossRef](#)]
49. Douglas, E.V.P.; Tom, L.B.; Ascher, D.B. pkCSM: Predicting Small-Molecule Pharmacokinetic and Toxicity Properties Using Graph-Based Signatures. *J. Med. Chem.* **2015**, *58*, 4066–4072.
50. Daina, A.; Michielin, O.; Zoete, V. SwissADME: A free web tool to evaluate pharmacokinetics, drug-likeness and medicinal chemistry friendliness of small molecules. *Sci. Rep.* **2017**, *7*, 42717. [[CrossRef](#)]
51. Abdel-Mohsen, H.T. Synthesis, crystal structure, and ADME prediction studies of novel imidazopyrimidines as antibacterial and cytotoxic agents. *Arch. Pharm.* **2020**, *353*, e1900271. [[CrossRef](#)]
52. Daina, A.; Zoete, V. A BOILED-Egg To Predict Gastrointestinal Absorption and Brain Penetration of Small Molecules. *ChemMed-Chem* **2016**, *11*, 1117–1121. [[CrossRef](#)] [[PubMed](#)]
53. Tong, L. Viral proteases. *Chem. Rev.* **2002**, *102*, 4609–4626. [[CrossRef](#)] [[PubMed](#)]
54. Hilgenfeld, R. From SARS to MERS: Crystallographic studies on coronaviral proteases enable antiviral drug design. *FEBS J.* **2014**, *281*, 4085–4096. [[CrossRef](#)] [[PubMed](#)]
55. Anand, K.; Ziebuhr, J.; Wadhwani, P.; Mesters, J.R. Coronavirus main proteinase (3CLpro) structure: Basis for design of anti-SARS drugs. *Science* **2003**, *300*, 1763–1767. [[CrossRef](#)]